Volume 56
Number 84
28 October 2020
Pages 12673–12870

# ChemComm

Chemical Communications

rsc.li/chemcomm

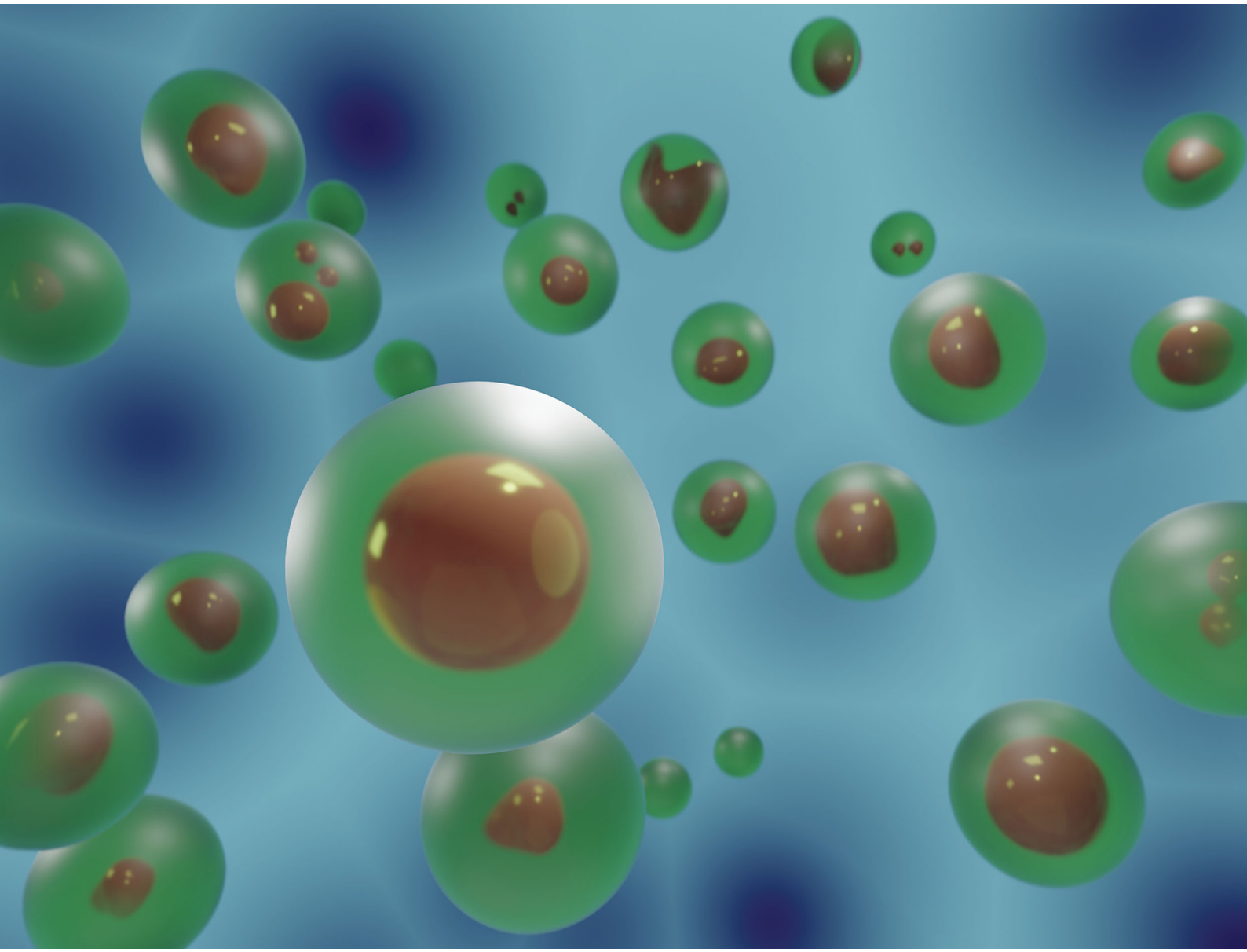

ISSN 1359-7345

ROYAL SOCIETY OF CHEMISTRY

**COMMUNICATION**

Stephen Mann *et al.*

Spontaneous membrane-less multi-compartmentalization *via* aqueous two-phase separation in complex coacervate micro-droplets

ChemComm

COMMUNICATION

View Article Online
View Journal | View Issue



Cite this: *Chem. Commun.*, 2020, **56**, 12717

Received 10th August 2020,
Accepted 10th September 2020

DOI: 10.1039/d0cc05399f

rsc.li/chemcomm



# Spontaneous membrane-less multi-compartmentalization *via* aqueous two-phase separation in complex coacervate micro-droplets†

Nicolette G. Moreau, [a] Nicolas Martin, [b] Pierangelo Gobbo, [a] T.-Y. Dora Tang [c] and Stephen Mann *[ade]

**Polyelectrolyte/nucleotide multiphase complex coacervate droplets are produced by internalized aqueous two-phase separation and used for the spatially dependent chemical transfer of sugar molecules, providing a step towards the development of membrane-free "organelles" within coacervate-based protocells.**

Liquid–liquid phase separated micro-droplets produced by complex coacervation between oppositely charged polyions represent promising platforms to elucidate essential features of prebiotic chemical organization and emulate membrane-less organelles found in living cells.[1,2] Coacervate droplets spontaneously sequester a wide range of functional solutes,[1,3–5] and have been reported to assist protein folding,[6] enhance enzyme activities[7] and transcription/translation rates,[8,9] and support RNA catalysis.[10,11] Coacervate droplets can also dynamically respond to pH,[1,12–15] temperature[16] or light,[17] but typically lack the morphological and functional heterogeneity of membrane-bounded protocell models. Significantly, membrane-less biological organelles have been reported to exhibit dynamic sub-structures including chemically-depleted vacuoles[18] and immiscible chemically-rich liquid domains,[19] which can facilitate sequential RNA processing by enzymes that localize in the distinct sub-compartments. Thus, achieving internal sub-structuration in synthetic coacervate droplets would provide a general strategy to spatially confine functional components into localized chemical reservoirs, dynamically segregate different biomolecules to distinct sub-compartments and orchestrate enzymatic reactions in space and time.

The formation of transient or stabilized water-filled vacuoles within complex coacervate droplets has been reported in association with osmotic pressure differences derived from *in situ* membrane formation,[20–22] in droplets exposed to a continuous electric field[23] and in the presence of a stoichiometric excess.[24] The spontaneous formation of multiphase-separated droplets in simple coacervates of elastin-like polypeptides[25] and in complex coacervates composed of multiple polyelectrolytes at equilibrium[26–28] has been recently reported.

In this paper, we show that coacervate micro-droplets prepared by electrostatic complexation of poly(diallyldimethylammonium chloride) (PDDA; 8500 g mol$^{-1}$, ~53 monomer units) and adenosine triphosphate (ATP; 25 mM, pH 8) undergo vacuolization upon addition of a low molecular weight neutral molecule, tetraethyleneglycol (TEG; HO[$CH_2CH_2O$]$_3CH_2CH_2OH$; 194.2 g mol$^{-1}$). Vacuole formation is attributed to strong partitioning of TEG in the coacervate phase and subsequent partial dehydration of the PDDA/ATP matrix. We further demonstrate that addition of both TEG and high molecular weight dextran reconfigures the PDDA/ATP droplets into multiphase complex coacervate droplets by segregative aqueous phase separation. Finally, we test whether TEG/dextran phase separation within the PDDA/ATP droplets can be used to implement the spatially dependent chemical transfer of sugar molecules within the droplets. We sequester dextranase specifically within the coacervate shell and exploit the *in situ* partial hydrolysis of the polysaccharide to generate oligosaccharide fragments that spontaneously partition into the TEG-containing PDDA/ATP matrix. Taken together, our results demonstrate that the formation of both chemically depleted (water-filled) vacuoles and chemically enriched sub-compartments in complex coacervate micro-droplets can be implemented by controlling the uptake and aqueous two-phase separation of incompatible neutral molecules within the molecularly crowded medium.

[a] *Centre for Protolife Research and Centre for Organized Matter Chemistry, School of Chemistry, University of Bristol, Bristol BS8 1TS, UK. E-mail: s.mann@bristol.ac.uk*
[b] *Univ. Bordeaux, CNRS, Centre de Recherche Paul Pascal, UMR5031, 115 Avenue du Dr Albert Schweitzer, 33600 Pessac, France*
[c] *Max Planck Institute of Molecular Cell and Genetics, Pfotenhauerstrasse 108, 01307 Dresden, Germany*
[d] *BrisSynBio Synthetic Biology Research Centre, Life Sciences Building, University of Bristol, Tyndall Avenue, Bristol, BS8 1TQ, UK*
[e] *Max Planck Bristol Centre for Minimal Biology, School of Chemistry, University of Bristol, Bristol BS8 1TS, UK*

† Electronic supplementary information (ESI) available: Details of experiments, optical and fluorescence microscopy images, phase diagram, partitioning data and supplementary movies. See DOI: 10.1039/d0cc05399f

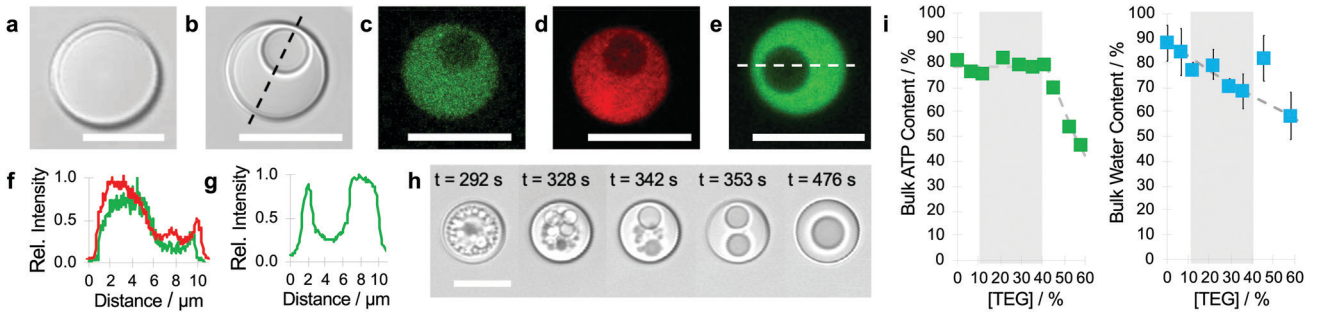


Fig. 1 (a and b) Brightfield microscopy images of single PDDA/ATP coacervate micro-droplets before (a) and after (b) addition of TEG showing the presence of a spherical vacuole within the TEG-containing droplets; scale bars, 10 μm. (c–e) Confocal fluorescent microscopy images showing the spatial distributions of ATP (c), PDDA (d) and TEG (e) specifically within the coacervate matrix of vacuole-containing single droplets. Fluorescence labels; TNP-ATP (green), RITC-PDDA (red), FITC-TEG (green). Scale bars, 10 μm. (f and g) Line profiles of fluorescence intensity across single droplets for TNP-ATP and RITC-PDDA (f) and FITC-TEG (g) showing depletion of ATP, PDDA and TEG in the vacuole. Profiles are recorded along the white dotted lines shown in (b) and (e), respectively. (h) Time series of brightfield microscopy images of TEG-induced vacuolization in a single droplet recorded at different times (see labels) after addition of TEG (22 wt%). (i) Plots of percentage ATP content compared to the total ATP added (left) and water content (right) of TEG-containing PDDA/ATP coacervate bulk phases as a function of TEG concentration. The percentage of ATP retained in the coacervate phase remains constant for TEG concentrations up to 42 wt%, after which vacuole formation no longer occurs. In contrast, the water content of the coacervate phase decreases linearly with increasing TEG concentration. The dotted lines indicate lines of best fit and the grey region identifies TEG concentrations compatible with vacuolization as determined by microscopy analysis. Error bars represents the standard deviation measured from three different samples.

Complex coacervate microdroplets were prepared as a turbid suspension of an equimolar charge ratio mixture of PDDA and ATP in water (see Methods). The droplets were approximately 10 μm in diameter and appeared spherical and structurally homogeneous when viewed by bright field optical microscopy after settling on a glass slide (Fig. 1a). Injection of TEG (final concentration, typically 22 wt%) or a mixture of TEG and fluorescein isothiocyanate (FITC)-labelled TEG into the supernatant at a remote distance (0.5 cm) gave rise to the spontaneous formation of a single sub-compartment of different optical density within each droplet typically after 5 min (Fig. 1b). Confocal fluorescence microscopy images of the TEG-containing coacervate droplets doped with 2,4,6-trinitrophenol (TNP)-tagged ATP, rhodamine-isothiocyanate (RITC)-labelled PDDA or FITC-TEG revealed that the vacuoles were water-filled and essentially free of ATP, PDDA and TEG (Fig. 1c–g). Formation of the vacuoles occurred *via* the nucleation and coalescence of multiple sub-micrometre-sized compartments within the coacervate droplets (Fig. 1h and Fig. S1, Video S1, ESI†). The vacuoles moved freely within the viscoelastic PDDA/ATP matrix, slowly decreased in size over time and were expelled irreversibly into the supernatant solution after 10–20 min. Vacuolization was observed by microscopy across a wide range of TEG concentrations (22–36 wt%; Fig. S2, ESI†) with an upper limit set by the TEG-induced destabilization of the PDDA/ATP coacervate droplets. Minimal changes in ATP concentration occurred during vacuole formation although the water content decreased linearly as the TEG concentration increased (Fig. 1i). Taken together, the above results indicated that high amounts of TEG (*ca.* 90% of added molecules) could be accumulated within the PDDA/ATP droplets without inducing major changes in the composition of the coacervate phase. The high level of partitioning was indicative of preferential interactions between the host and guest components, which in turn resulted in microphase separation to produce water-filled vacuoles possibly *via* volume exclusion effects, decreases in water activity and surface tension changes coupled to dehydration of the polyionic complexes in the coacervate phase by osmotic pressure.[29–31]

Given the ability of TEG to induce vacuolization within the PDDA/ATP coacervate droplets and undergo segregative liquid–liquid phase separation in the presence of high molecular weight dextran (Fig. S3, ESI†),[32] we sought to exploit these processes to replace the molecularly depleted water-filled vacuoles with a chemically enriched sub-compartment. In so doing, we aimed to develop a spontaneous pathway to spatially organized droplets based on the confinement of aqueous two-phase separation within the matrix of an electrostatically matched complex coacervate. To achieve this goal, we mounted the PDDA/ATP coacervate droplets under water on a glass slide, added dextran (final concentration, 1.2 mg $mL^{-1}$) with a molecular weight of 70 or 150 kDa, and then injected TEG (final concentration, 6 wt%) into the supernatant. Doping the coacervate droplets with TNP-ATP and RITC-PDDA and using unlabelled or fluorescently labelled TEG and dextran revealed the presence of a single well-defined sub-compartment in each droplet that was enriched in dextran and surrounded by a coacervate matrix containing ATP, PDDA and TEG (Fig. 2a–c). The free-moving dextran sub-compartments were stable within the coacervate droplets and were not readily expelled into the supernatant. Interestingly, real-time confocal fluorescence microscopy revealed that high molecular weight dextran was initially excluded from the coacervate droplets (Fig. S4, ESI†) and did not induce vacuolization. In contrast, when TEG was added rapidly ($t < 13$ s) to a dextran-containing suspension of PDDA/ATP droplets, the uniform partitioning of the oligoether into the coacervate phase triggered the uptake of dextran into the coacervate phase. Time-dependent fluorescence microscopy images revealed droplets that initially contained a homogeneous

 

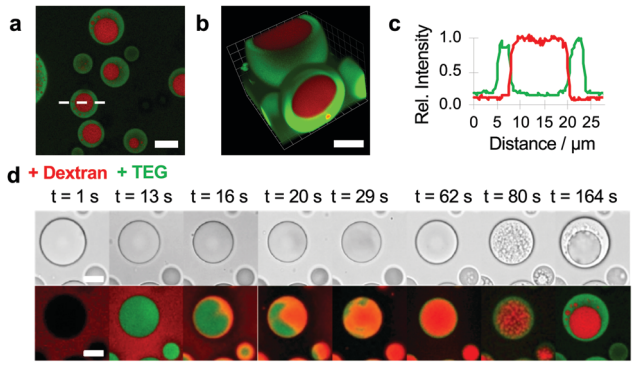


Fig. 2 (a–c) Confocal fluorescence microscopy (a) and 3D reconstruction (b) images, and fluorescence line profiles recorded across a single droplet (c) (white dashed line in (a)) showing demixing and subsequent spatial segregation of TEG (FITC-TEG, green fluorescence) and dextran (RITC-dextran, red fluorescence) within individual PDDA/ATP coacervate micro-droplets. Internalized aqueous two-phase separation occurs after addition of TEG to a suspension of droplets containing non-partitioned dextran, resulting in a dextran-enriched sub-compartment and surrounding TEG-loaded coacervate matrix. (Dextran final concentration, 1.2 mg $mL^{-1}$, molecular weight, 70 or 150k; TEG 6 wt%). Scale bars, 10 μm. (d) Time series of bright field (top row) and corresponding confocal fluorescence (bottom row) microscopy images of an individual coacervate droplet showing formation of an internal dextran (RITC-dextran)-rich sub-compartment (red fluorescence) after addition of TEG/FITC-TEG. Addition of dextran in the absence of TEG results in exclusion of the polysaccharide (see $t$ = 1 s). Subsequent injection of TEG results in sequestration of the oligoether ($t$ = 13 s), followed by influx of dextran and mixing within the PDDA/ATP coacervate phase ($t$ = 16–62 s). Multiple dextran-enriched nuclei are then produced by internalized TEG/dextran demixing ($t$ = 80 s) followed by coalescence to produce a single dextran sub-compartment surrounded by a TEG-containing coacervate matrix ($t$ = 164 s). The asymmetric uptake of dextran follows the TEG diffusion gradient produced by injection of TEG from one side (right side in the viewed images) of the glass slide. Dextran final concentration 1.2 mg $mL^{-1}$, molecular weight, (70k; TEG, 6 wt%). Scale bars, 5 μm.

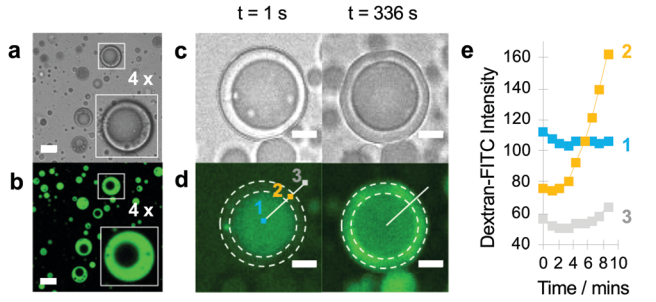


Fig. 3 Bright field (a) and confocal fluorescence (b) microscopy images of PDDA/ATP coacervate micro-droplets doped with FITC-dextranase (green) after sequential addition of dextran (70 kDa; final concentration, 1.2 mg $mL^{-1}$) and TEG (final concentration, 6 wt%) showing preferential partitioning of the enzyme into the TEG-containing coacervate. The non-fluorescent sub-compartments contain phase-separated dextran. Insets show ×4 magnified images of a single coacervate droplet (see white box). Scale bars, 10 μm. Brightfield (c) and confocal (d) fluorescent images of a single coacervate droplet doped with dextranase, which resides in the outer coacervate rich compartment, after sequential addition of FITC-dextran (70 kDa, 1.2 mg $mL^{-1}$ final concentration) and TEG (6 wt% final concentration). The dextran-rich compartment (1), the coacervate-rich compartment (2) and the outside aqueous phase (3) are indicated by dotted circles. In the presence of dextranase at the interface between the inner and outer compartment, high molecular weight dextran is converted into lower molecular weight species which are then sequestered into the outer coacervate region (2) ($t$ = 336 s). Scale bars, 5 μm. (e) Plot of fluorescence intensity values measured at radial distances 1, 2 and 3 as marked in $c$ plotted against time. An increase in fluorescence intensity is seen in the coacervate region (2), indicating movement of FITC-dextran through the different regions.

mixture of TEG and dextran, but which spontaneously demixed with time *via* aqueous two-phase separation to produce randomly distributed dextran-enriched nuclei that coalesced into a single dextran sub-compartment entrapped within the TEG-containing coacervate matrix (Fig. 2d and Fig. S5, Video S2, ESI†). Reducing the concentration of dextran inhibited coalescence of the incipient phase-separated nuclei to produce coacervate droplets with multiple quasi-stable sub-compartments (Fig. S6, ESI†). No dextran/TEG phase separation was observed within the droplets when a low molecular weight (4 kDa) dextran was used even though dextran was partitioned within the droplets in the absence of TEG (Fig. S7, ESI†).

We tested whether TEG/dextran phase separation within the PDDA/ATP droplets could be used to implement the spatially dependent enzyme-mediated chemical transfer between the sub-compartment and surrounding coacervate matrix. As low molecular weight dextran was preferentially partitioned in the coacervate phase (Fig. S4, ESI†), we used *in situ* enzyme-mediated hydrolysis of the dextran sub-compartment to displace low molecular fragments of the polysaccharide reservoir into the enclosed TEG-containing coacervate matrix. To achieve this, we partitioned dextranase specifically into the TEG-enriched coacervate phase of droplets (Fig. 3a and b), and then monitored the localization and displacement of the polysaccharide fragments by using FITC-labelled dextran (70 kDa) as the guest molecule. Fluorescence microscopy images showed a progressive displacement of the green fluorescence intensity from the phase-separated sub-compartment to the coacervate phase typically within 5 min (Fig. 3c and d), which was consistent with line profiles recorded across individual droplets (Fig. 3e). We attributed these observations to the onset of dextranase-mediated partial hydrolysis of the polysaccharide chains into fluorescently tagged oligosaccharides, which in turn diffused across the phase boundary into the surrounding coacervate phase.

Taken together, our results demonstrate the ability of a small neutral molecule (TEG) to spontaneously induce the formation of multiphase complex coacervate droplets comprising water-filled vacuoles or dextran-enriched sub-compartments. Vacuolization occurs for added TEG concentrations between 22–36 wt% and is attributed to the coupling of changes in surface tension to partial dehydration of the PDDA/ATP coacervate phase by osmotic pressure. Interestingly, addition of either tetraethylene glycol monomethyl ether (TEG–$CH_3$) or tetraethylene glycol dimethyl ether ($CH_3$–TEG–$CH_3$) did not induce vacuolization (Fig. S8, ESI†), suggesting that TEG-induced formation of the vacuoles was predominantly driven by hydrogen bonding and not hydrophobic interactions. In the presence of non-partitioned dextran, addition of low levels of TEG (6 wt%) to the continuous phase gives rise to co-sequestration followed by aqueous two-phase separation of the

guest molecules to give a freely moving dextran sub-compartment embedded within a TEG-containing coacervate matrix. Interestingly, uptake of dextran is only initiated after the transfer of TEG from the continuous phase, suggesting that repulsive interactions between the PDDA/ATP matrix and polysaccharide macromolecules are attenuated in the presence of the oligoether. Moreover, as the concentrations of sequestered TEG and dextran are initially low, uptake of the guest molecules at first generates a homogeneous mixture within the droplets, which becomes unstable over time as the sequestered concentrations progressively increase. As the experimentally derived TEG partition coefficient at 6 wt% is approximately 14, we estimated a mean final concentration of TEG within the droplets of 3.6 M (coacervate volume fraction, 0.7%). Given this high level of sequestration, internalized demixing should occur once the dextran concentration attains a minimal value of 3 mg $mL^{-1}$ (see Fig. S3, ESI†), equivalent to partitioning of approximately only 1.6% of the added dextran. Interestingly, no internalized segregative phase separation was observed when TEG was initially sequestered into the droplets followed by addition of high molecular weight dextran (Fig. S9, ESI†). Under these conditions, the dextran remained excluded from the droplet interior, presumably due to the high levels of preloaded TEG that inhibited mixing at the droplet/water interface.

Demixing of neutral molecules within the molecularly crowded complex coacervate at first sight seems surprising given the highly charged nature of the milieu but can be attributed to the reduced dielectric constant of the PDDA/ATP matrix,[1] and the high level of incompatibility between the guest molecules.[31] These factors also facilitate the sequestration of dextranase specifically into the TEG-containing molecular crowded matrix rather than the polysaccharide-enriched subcompartment, and as a consequence enables the spatially dependent chemical transfer of sugar molecules within the multiphase droplets. This strategy offers a means to control the displacement of the internal reservoir across the internal phase boundary and could provide a route to the development of chemically dynamic ''organelles'' within coacervate-based protocell models.

In conclusion, our results demonstrate a simple and robust approach to spontaneous sub-compartmentalization within synthetic coacervate micro-droplets by rationally exploiting internalized processes of liquid–liquid phase separation. The work highlights new opportunities for the multi-phase restructuring of complex coacervate droplets and could provide a step towards the development of protocell models with subdivided interiors capable of programmable chemical trafficking.

This work was supported by the EPSRC (EP/G036780/1; Bristol Centre for Functional Nanomaterials), the ERC Advanced Grant Scheme (EC-2016-ADG 740235), BrisSynBio (BB/L01386X/1) and MaxSynBio Consortium (jointly funded by the Federal Ministry of Education and Research (Germany) and the Max Planck Society). We thank Dr S. Briggs for help with the preparation of RITC-PDDA.

## Conflicts of interest

There are no conflicts to declare.

## Notes and references

1 S. Koga, D. S. Williams, A. W. Perriman and S. Mann, *Nat. Chem.*, 2011, **3**, 720–724.
2 N. Martin, *ChemBioChem*, 2019, **20**, 2553–2568.
3 D. S. Williams, S. Koga, C. R. C. Hak, A. Majrekar, A. J. Patil, A. W. Perriman and S. Mann, *Soft Matter*, 2012, **8**, 6004–6014.
4 T.-Y. D. Tang, M. Antognozzi, J. A. Vicary, A. W. Perriman and S. Mann, *Soft Matter*, 2013, **9**, 7647–7656.
5 E. A. Frankel, P. C. Bevilacqua and C. D. Keating, *Langmuir*, 2016, **32**, 2041–2049.
6 N. Martin, M. Li and S. Mann, *Langmuir*, 2016, **32**, 5881–5889.
7 J. Crosby, T. Treadwell, M. Hammerton, K. Vasilakis, M. P. Crump, D. S. Williams and S. Mann, *Chem. Commun.*, 2012, **48**, 11832–11834.
8 E. Sokolova, E. Spruijt, M. M. K. Hansen, E. Dubuc, J. Groen, V. Chokkalingam, A. Piruska, H. A. Heus and W. T. S. Huck, *Proc. Natl. Acad. Sci. U. S. A.*, 2013, **110**, 11692–11697.
9 T.-Y. D. Tang, D. van Swaay, A. deMello, J. L. R. Anderson and S. Mann, *Chem. Commun.*, 2015, **51**, 11429–11432.
10 B. Drobot, J. M. Iglesias-Artola, K. Le Vay, V. Mayr, M. Kar, M. Kreysing, H. Mutschler and T.-Y. D. Tang, *Nat. Commun.*, 2018, **9**, 3643.
11 R. R. Poudyal, R. M. Guth-Metzler, A. J. Veenis, E. A. Frankel, C. D. Keating and P. C. Bevilacqua, *Nat. Commun.*, 2019, **10**, 490.
12 D. Garenne, L. Beven, L. Navailles, F. Nallet, E. J. Dufourc and J.-P. Douliez, *Angew. Chem., Int. Ed.*, 2016, **55**, 13673–13677.
13 J. P. Douliez, N. Martin, C. Gaillard, T. Beneyton, J.-C. Baret, S. Mann and L. Beven, *Angew. Chem., Int. Ed.*, 2017, **56**, 13689–13693.
14 N. Martin, J.-P. Douliez, Y. Qiao, R. Booth, M. Li and S. Mann, *Nat. Commun.*, 2018, **9**, 3652.
15 C. Love, J. Steinkühler, D. T. Gonzales, N. Yandrapalli, T. Robinson, R. Dimova and T.-Y. D. Tang, *Angew. Chem., Int. Ed.*, 2020, **59**, 5950.
16 W. M. Aumiller Jr, F. P. Cakmak, B. W. Davis and C. D. Keating, *Langmuir*, 2016, **32**, 10042–10053.
17 N. Martin, L. Tian, D. Spencer, A. Coutable-Pennarun, J. L. R. Anderson and S. Mann, *Angew. Chem., Int. Ed.*, 2019, **58**, 14594–14598.
18 H. B. Schmidt and R. Rohatgi, *Cell Rep.*, 2016, **16**, 1228–1236.
19 M. Feric, N. Vaidya, T. S. Harmon, D. M. Mitrea, L. Zhu, T. M. Richardson, R. W. Kriwacki, R. V. Pappu and C. P. Brangwynne, *Cell*, 2016, **165**, 1686–1697.
20 D. W. Williams, A. J. Patil and S. Mann, *Small*, 2014, **10**, 1830–1840.
21 L. Tian, M. Li, A. J. Patil, B. W. Drinkwater and S. Mann, *Nat. Commun.*, 2019, **10**, 3321.
22 P. Gobbo, L. Tian, P. B. V. V. S. Kumar, S. Turvey, M. Cattelan, A. J. Patil, M. Carraro, M. Bonchio and S. Mann, *Nat. Commun.*, 2020, **11**, 41.
23 Y. Yin, L. Niu, X. Zhu, M. Zhao, Z. Zhang, S. Mann and D. Liang, *Nat. Commun.*, 2016, **7**, 10658.
24 P. R. Banerjee, A. N. Milin, M. M. Moosa, P. L. Onuchic and A. A. Deniz, *Angew. Chem., Int. Ed.*, 2017, **56**, 11354–11359.
25 J. R. Simon, N. J. Carroll, M. Rubinstein, A. Chilkoti and G. P. Lopez, *Nat. Chem.*, 2017, **9**, 509–515.
26 G. A. Moutain and C. D. Keating, *Biomacromolecules*, 2020, **21**, 630–640.
27 T. Lu and E. Spruijt, *J. Am. Chem. Soc.*, 2020, **142**, 2905–2914.
28 T. Kojima and S. Takayama, *ACS Appl. Mater. Interfaces*, 2018, **10**, 32782–32791.
29 A. M. Marianelli, B. M. Miller and C. D. Keating, *Soft Matter*, 2018, **14**, 368–378.
30 H. H. Hariri, A. M. Lehaf and J. B. Schlenoff, *Macromolecules*, 2020, **45**, 9364–9372.
31 M. Gao, D. Gnutt, A. Orban, B. Appel, F. Righetti, R. Winter, F. Narberhaus, S. Muller and S. Ebbinghaus, *Angew. Chem., Int. Ed.*, 2016, **55**, 3224–3228.
32 C. D. Keating, *Acc. Chem. Res.*, 2012, **45**, 2114–2124.

 